Research Article

Automated detection and characterization of graphene and few-layer graphite via Raman spectroscopy

J. M. Caridad,[a,b] F. Rossella,[a] V. Bellani,[a*] M. S. Grandi[a] and E. Diez[b]

Several processes have to be automated in order to use graphene in future industrial applications. One of these is the detection and characterization of graphene and few-layer graphite (FLG) flakes on a substrate. Raman spectroscopy is an ideal tool for this purpose, as it allows not only the identification of these graphitic materials on arbitrary substrates but also monitoring the quality of flakes within the sample. In this paper, we report how graphene and FLG crystallites can be automatically detected and characterized by monitoring the evolution of Raman bands. We present an algorithm that achieves this purpose and thus has special potential in industrial applications of graphene. Copyright © 2010 John Wiley & Sons, Ltd.

Keywords: Raman spectroscopy; graphene; automated detection

Introduction

Consisting of one monolayer of carbon atoms structured in a honeycomb lattice, graphene is the most recently discovered carbon allotrope.[1] Because of its novel properties,[2] much effort is devoted to its study.[3] Several methods have been reported in the literature to prepare graphene, such as micromechanical cleavage,[1] epitaxial growth,[4,5] chemical vapor deposition[5,6] or chemical exfoliation.[7] These techniques can in principle create not only graphene but all sorts of carbon species like flakes consisting of few-layer graphite (FLG) or bulk graphite. Consequently, locating possible graphene or FLG fragments within the sample is a time-consuming process. The large number of technological applications in which this novel material can be employed[8–11] requires to speed up the detection and characterization process of graphene and FLG. Therefore, the automation of fast and robust visualization techniques is highly desirable within this emerging area.

Several methods have been described in the literature for detecting and characterizing graphene and FLG, which can be grouped into optical microscopy, scanning probe microscopy and photon scattering. Visualization via optical microscopy allows a fast survey of large areas. The identification is either performed by observing the contrast between graphene and the substrate[8,12–14] or by a total color difference method.[15] Both techniques depend on the thickness and optical properties of an intermediate dielectric layer placed between graphene (or FLG) and the substrate. This technique exploits an appropriate substrate and dielectric film to unambiguously characterize graphene and FGL crystallites; thus, it cannot be used in the fabrication of graphene-based devices on arbitrary substrates. Scanning probe identification tools provide atomic-scale resolution despite of a low throughput. Atomic force microscopy (AFM) is commonly used to measure the thickness of graphene and FLG[1,16,17]; however, the literature reports certain deviation in thicknesses values, which suggests a dependence on experimental laboratory conditions, sample preparation or both.[18] Scanning tunneling microscopy (STM) and transmission electron microscopy (TEM) can detect structural ripples of nanosized graphene,[19,20] but STM requires an extra measurement (typically AFM or Raman spectroscopy) to identify graphene[21] and TEM is a destructive technique.[17] Finally, scanning electron microscopy (SEM) allows distinguishing FLG from thicker graphitic flakes,[22] although this method is not viable for identification due to the introduction of a contaminant layer on the exposed area.[14] Detection tools based on photon scattering are important to obtain information about the structural properties of matter. Raman spectroscopy by itself, or a combination Raman and Rayleigh spectroscopy, is the main technique used to detect graphene and FLG.[16,17,23,24] Raman spectra provide clear detection of graphene and FLG and also achieve information about graphene edges,[25–27] doping[28–30] and defects.[30] The papers cited above present Raman results for graphene and FLG flakes grown on Si with a SiO$_2$ thin dielectric layer; nevertheless, recent studies show that this technique is also applicable on arbitrary substrates.[31,32] A detection procedure faster than Raman imaging to find graphene and FLG is achieved by combining Rayleigh and Raman spectroscopies.[17] Both measurements can be done at the same time using a notch filter to reduce the elastically scattered light. Considering the previous arguments, the combined Raman–Rayleigh or only Raman techniques appear to be two appropriate tools to efficiently automate the location and characterization of graphene and FLG. However, in the former method, i.e. when the two techniques are merged, the microscope has to be set up properly to avoid charge-coupled device (CCD) saturation because of the Rayleigh band intensity (even with a notch filter placed before the CCD, this signal still remains greater

* Correspondence to: V. Bellani, CNISM – Dipartimento di Fisica 'A. Volta', Università di Pavia, Pavia, Italy. E-mail: bellani@unipv.it

a CNISM – Dipartimento di Fisica 'A. Volta', Università di Pavia, Pavia, Italy

b Laboratorio de Bajas Temperaturas, Facultad de Ciencias Físicas, Universidad de Salamanca, Salamanca, Spain

that the Raman fingerprints). In this way, it is not easy to detect weaker Raman bands and therefore difficult to obtain some extra information about graphene (or FLG).

In this work, we report how an automatic detection and characterization of graphene and FLG crystallites can be performed by examining the Raman spectra. We confirm the validity of this algorithm using AFM measurements. The paper is organized as follows: in the section 'Experimental' we present the experimental details; in the section 'Results and Discussion' we illustrate Raman fingerprints as an identification tool for graphene and FLG; from this discussion, we suggest in the section 'An algorithm for graphene and FLG characterization' a fast, efficient and robust algorithm that achieves the proposed goal. Finally, the section 'Conclusion' contains conclusions and perspectives for future work.

Experimental

Graphene and FLG were prepared using micromechanical cleavage (and independently characterized) by the company Graphene Industries. The substrate employed is (100)-oriented Si with an approximately 300 nm dry thermal SiO_2 thin film. Figure 1 shows the optical images of the two samples used for this work (containing graphene, bilayer and trilayer graphite). The difference in the color between Fig. 1(a) and (b) is due to the thickness of SiO_2 layer and is perceptible also in zones without graphene or FLG. Really, because of interference effects, the color of SiO_2 on Si depends on the thickness of SiO_2 film, which is between 280 and 310 nm. For these thicknesses, the color of the wafer varies from violet/blue to blue, and this explains the two colors that we observe in Fig. 1(a) and (b).[33]

Raman scattering measurements were carried out with a micro-Raman spectrometer (Horiba Jobin-Yvon apparatus) using a 100× objective (laser spot ~1 μm^2). The instrument spectral resolution was approximately 2 cm^{-1} and the employed laser excitation wavelength was 632.81 nm. A notch filter was installed before the CCD detector to stop the laser light. Accurate calibration was carried out by checking the Rayleigh band and Si band at 0 and 520.7 cm^{-1}, respectively. All experiments were performed at room temperature. The measured areas were scanned with a spatial resolution of approximately 0.5 μm. The acquisition time used for all the positions was of the order of a few minutes (from 1 to 3 min in the mappings presented here), and power on the samples was below 1 mW to avoid heating and to preserve the sample.[34] We undertook AFM measurements with a Digital Instruments MMAFM-2 equipment. The atomic force micrographs were made in tapping mode using diamond-like carbon coated tips with a nominal radius of 15 nm.

Results and Discussion

Raman imaging and Lorentzian deconvolution as graphene and FLG identification tools

The so-called G, D and two-dimensional (2D) bands are the three principal Raman features in carbon allotropes,[23] which lie in graphite at approximately 1580, 1300 and 2700 cm^{-1}, respectively. The G band corresponds to the E_{2g} phonon at the Brillouin zone center, the D peak is due to the collective breathing modes of rings within the graphene lattice[35] and the 2D peak is the second order of D line.[23] By the imaging parameters of the Raman bands, the detection and characterization of graphene
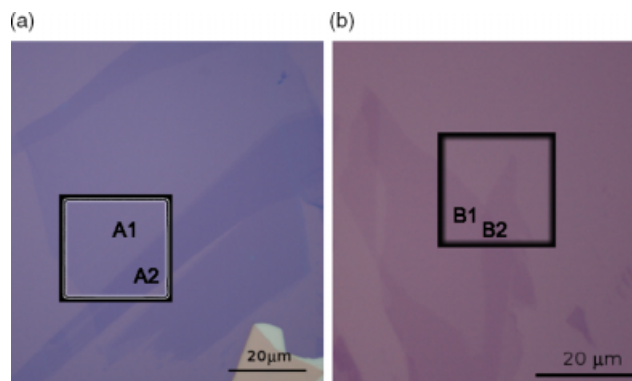

Figure 1. Optical microscope images of the studied areas. (a) Graphene (A1) and three-layer graphite (A2); graphene zone has two small 'cuts' as we will detect later on Raman mappings. (b) Graphene (B1) and two-layer graphite (B2). The substrate for both samples is Si with a 300-nm SiO_2 thin film.

or FLG can be achieved.[16,24,25] Moreover, through G, D and 2D Raman modes, valuable information can be extracted such as the quality of graphene and FLG layers,[30] intrinsic doping due to the substrate,[28] temperature[34] and strain exhibited in the sample.[36] Nevertheless, special problems arise when attempting to automatically perform these tasks (noise spikes in the measurement registered by the CCD, stability of laser intensity, unintentional impurities within the sample, defects, etc.). In the following paragraphs, we illustrate and discuss the information from G, 2D and D bands that can be used to detect and characterize graphene.

G band

Figure 2 shows Raman imaging from the area selected in Fig. 1(a) depending on four parameters: G peak intensity [IntPeak(G)], G band integrated intensity [Int(G)], G band full width at half maximum [FWHM(G)] and G peak shift [Pos(G)]. A distinction between the number of stockpiled graphene sheets can be achieved by considering IntPeak(G). (Note that this parameter cannot determine absolutely by itself whether an area is graphene, FLG or bulk graphite; it allows the discrimination among graphene layers by comparison.) This parameter increases linearly with increasing number of layers in FLG. As seen in Fig. 2(a), IntPeak(G) presents some fluctuations inside graphene (or FLG) regions; however, those variations are much smaller compared to the change among the different zones. Furthermore, graphene edges and FLG edges can be detected as well through the changes in intensity levels at the borders. The main disadvantage of this parameter is that it is very sensitive to the presence of spurious noise spikes. By imaging the integrated intensity of the G band, i.e. Int(G), areas with graphene or FLG can be differentiated (Fig. 2(b)). Despite of the slight degradation of its value due to doping,[37] Int(G) grows almost linearly up to nine layers approximately.[38] This behavior makes this parameter suitable for locating and characterizing graphene and FLG by comparison with different positions. Moreover, Int(G) is almost insensitive to the presence of noise spikes (the latter have much smaller areas than Int(G)). FWHM(G) imaging (Fig. 2(c)) should not be used to characterize graphene. It does not exhibit any substantial change for graphene and FLG.[30] Furthermore, this parameter varies depending on the impurity concentration (for higher concentrations, the G band FWHM decreases).[28,37] Pos(G) shifts toward lower wavenumbers
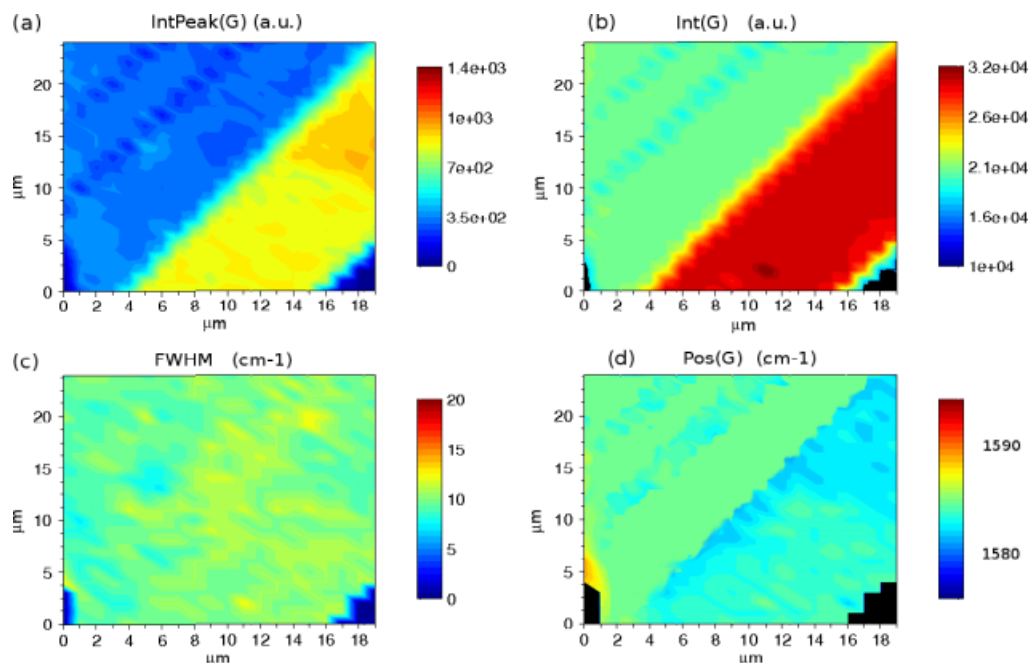
Figure 2. G band Raman imaging. The number of graphene layers can be clearly identified by comparison using IntPeak(G) (a) and Int(G) (b). FWHM(G) (c) and Pos(G) (d) undergo considerable changes with doping, making these two parameters unsuitable for characterizing graphene (FLG).
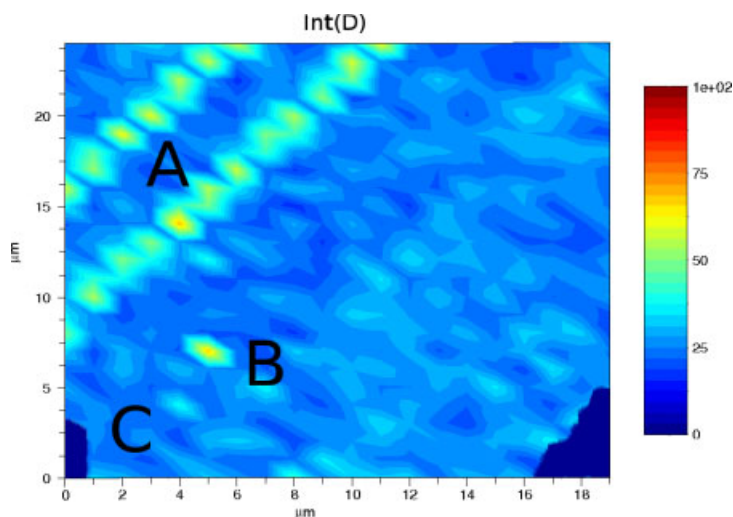

Figure 3. D peak integrated intensity. Under circular laser polarization, D band is active near the borders due to the presence of armchair edge or disorder (zone A), or in the defective regions in the middle of the graphene area (zone B). It can be appreciated how in edges without disorder and with zigzag chirality, the D band is not active (zone C).

with increasing number of graphene sheets (Fig. 2(d)). Pos(G) is dependent on the substrate on which graphene (or FLG) is grown[23,32] and shifts when graphene is doped,[28,37] making this parameter unsuitable for characterizing graphene or FLG.

D band

Under circular laser polarization, the D band appears in the presence of defects in graphene and FLG[30] or when armchair chirality or defects are present at the borders.[25–27] The value of D band integrated intensity, Int(D), is proportional to the amount of armchair or defects that exists within the laser spot area. Figure 3 shows an imaging of Int(D). We can observe that some positions on graphene edges have an intense D band, indicating the presence

of armchair edge or disorder. Moreover, there are positions not located on the border with considerable Int(D), due only to defects in graphene (or FLG).

2D band

Graphene and FLG identification can be obtained using 2D Raman band as well.[30] This process can be achieved in two different ways: (1) by fitting the band through Lorentzian deconvolution and (2) by comparing the band parameters of neighboring positions. Concerning method (1), we mention that the graphene 2D line is a single, sharp Lorentzian peak and bilayer graphite has four Lorentzian components,[30] while a recent work[39] shows that trilayer graphite has nine optical processes that contribute to the
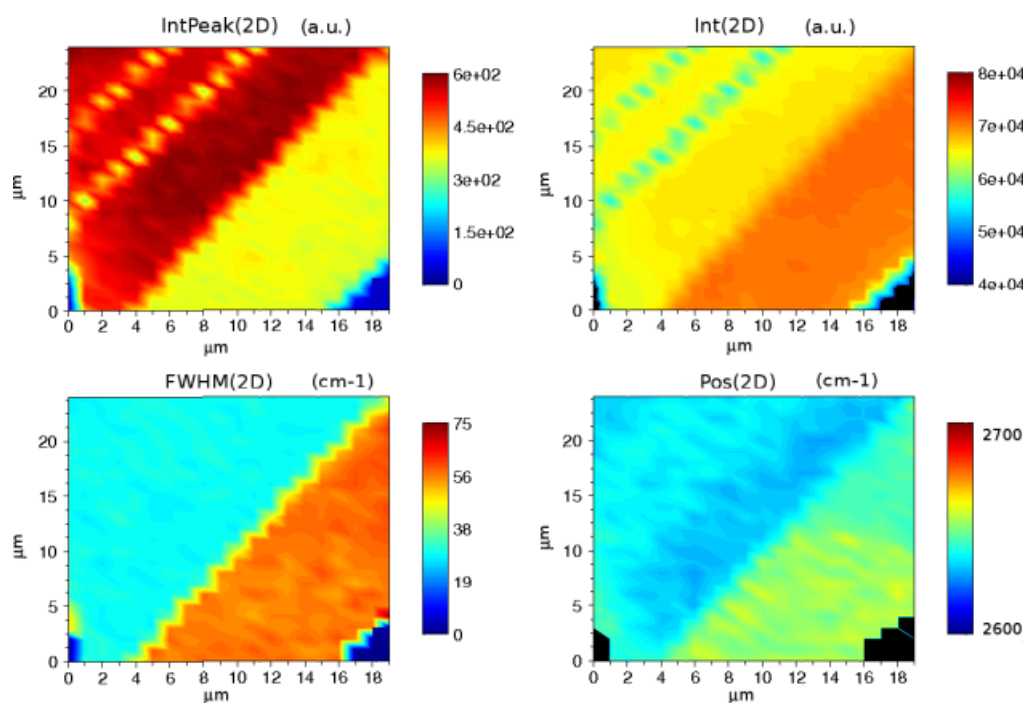
Figure 4. 2D band Raman imaging obtained by comparing the band parameters of neighboring positions. IntPeak(2D) (a), Int(2D) (b), FWHM(2D) (c) can clearly distinguish between graphene and FLG. This is due to graphene having a single Lorentzian peak, whereas for FLG the 2D band is the convolution of several peaks. However, the 2D band does not provide a clear identification among different FLGs.

2D band. To date, the Lorentzian deconvolution for more than three graphene layers has not been reported, but the 2D line has been commonly fitted using two peaks as for bulk graphite.[16,24] Thus, graphene and FLG characterization using 2D band fitting is a direct and robust identification method, as it does not need comparisons among neighboring positions; however, 2D peak fitting can provide unambiguous characterization only up to three-layer graphite. Moreover, method (1) is time consuming due to the computational work to deconvolute a 2D band into the corresponding Lorentzian components. In this work, 2D band fittings for graphene, bilayer and trilayer graphite were undertaken only when necessary, using the methods explained by Dresselhaus and coworkers.[39,40] Fig. 4 shows the 2D band Raman imaging of the region selected in Fig. 1(a) obtained using method (2), where the different zones in the mapped area have been differentiated by comparing the band parameters of neighboring positions. Especially appreciable are the differences between graphene and FLG imaged 2D band peak intensity [IntPeak(2D)], integrated intensity [Int(2D)] and FWHM(2D).

However, this comparison method does not provide significant changes among FLGs; therefore, we do not compare 2D band values to characterize graphene and FLG in this work. As regards graphene purity, Fig. 5 presents three Raman imagings which can be used to monitor the quality of the sample. Figure 5(a) reports D peak integrated intensity $I(D)$ (only for the graphene region). As stated before, the D peak is activated by disorder and increases with its amount.[28,37] Fig. 5(b) and (c) shows doping concentration in the sample by imaging two different ratios: Pos(G)/FWHM(G) and $I(2D)/I(G)$, respectively. Doping in graphene is induced by unintentional impurities on the substrate and by absorbates.[28] For higher doping concentrations, Pos(G) increases, FWHM(G) decreases, $I(2D)$ decreases and $I(G)$ increases.[28,37] Thus, for higher doping concentrations, the ratios Pos(G)/FWHM(G) and

$I(2D)/I(G)$ will increase and decrease, respectively. These behaviors are clearly shown in Fig. 5(b) and (c). Both figures agree and, in this case, it can be appreciated how high doping areas such A and B are near the border.

Finally, we used AFM to confirm the validity of the Raman results. The thicknesses measured by AFM of the different zones which appear in the selected areas of Fig. 1 are as follows: 0.9 ± 0.3 nm for region A1, 2.8 ± 0.2 nm for A2, 0.8 ± 0.3 nm for B1 and 1.7 ± 0.3 nm for B2 (values are averaged among five random positions within each area). Comparing this data with previous studies,[17,18,24] we verify that the selected region in Fig. 1(a) is composed by a graphene monolayer and three-layer graphite, while the chosen area in Fig. 1(b) contains graphene and bilayer graphite.

An algorithm for graphene and FLG characterization

Having illustrated the main Raman features that can be used to detect and characterize graphene and FLG, we present an algorithm that automatically and efficiently achieves this purpose. The flowchart of the algorithm is shown in Figs 6 and 7. The general algorithm is presented in Fig. 6, and it can be divided into five blocks:

(1) Reading of the Raman spectra.
(2) Detection of a graphene position within Raman spectra fitting 2D band. If graphene is not found, the process would go on fitting bilayer graphite. Then, if no bilayer graphite is detected, the process would be repeated for trilayer graphite. Eventually, if no trilayer graphite is encountered, 2D band cannot unambiguously differentiate the rest of FLG, and therefore only G, D and 2D band imaging results will be the outcome of the algorithm.
(3) If graphene, bilayer or trilayer graphite are found in some position, the G band integrated intensity is calculated
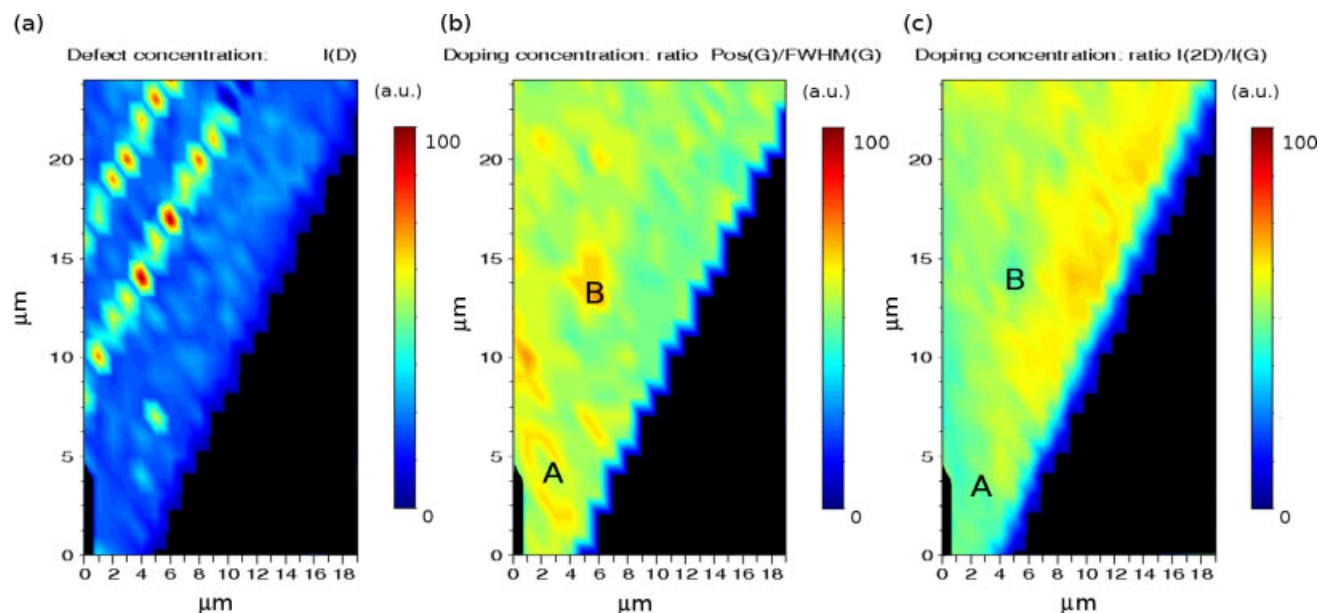
Figure 5. Graphene defects and impurity concentration. Defects are monitored by D peak intensity I(D) (a), and doping levels through the ratios Pos(G)/FWHM(G) and I(2D)/I(G) (b and c). Both ratios increase and decrease, respectively, when the impurity concentration increases.
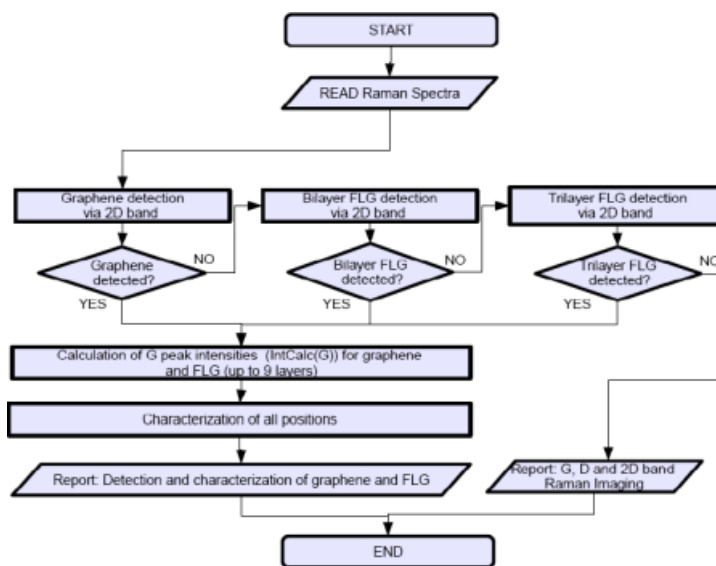

Figure 6. General flowchart of the algorithm.

[IntCalc(G)] up to nine layer graphite, since, for FLG, Int(G) grows linearly with the number of the graphene layers.[38] The characterization of the rest of the positions is done comparing the difference IntCalc(G) - Int(G) with an offset, which is defined by the user when calibrating the experimental conditions.

(4) The algorithm performs the routine successively to characterize all the positions, as described in Fig. 7.

(5) Finally, the program produces an image showing the characterization of all the zones within the imaged area.

The algorithm's core is the subroutine that characterizes all the mapped positions depending on their Raman spectra. Its flowchart is illustrated in Fig. 7. This routine takes Raman spectra and the previously calculated IntCalc(G) as inputs. It can be split into three main blocks:

(i) First, Int(G) is compared with the calculated values IntCalc(G). If Int(G) matches with any of IntCalc(G) (for a certain tolerance chosen by the user), the position is characterized with the corresponding number of layers.

(ii) If Int(G) does not match with any IntCalc(G), the routine checks whether the position is a border position graphene-substrate (Int(G) < IntCalc(G) of graphene; 2D band can be fitted to one single Lorentzian peak). In the affirmative case (the position is a border between graphene and substrate), Int(D) will discriminate the presence or absence of armchair/disordered edge in that particular position. In the negative case, there is a contradiction between G and 2D band parameters and the routine will output an 'uncharacterized position' (The 'uncharacterized position' case is obtained either under abnormal situations (high disorder, considerable spikes in
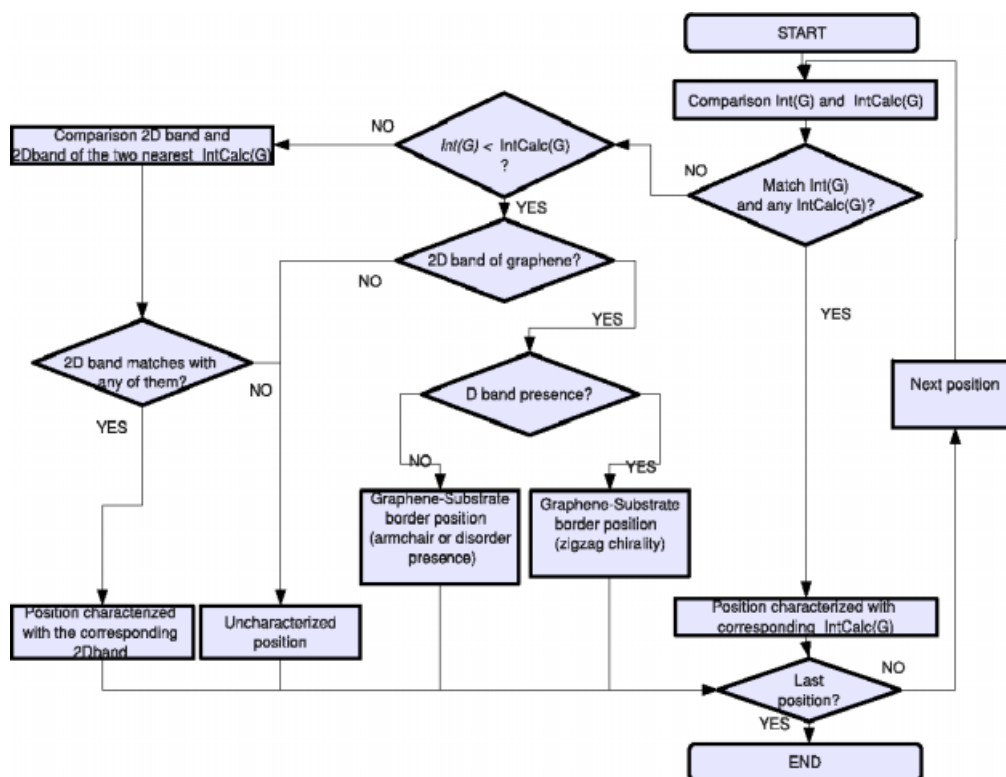
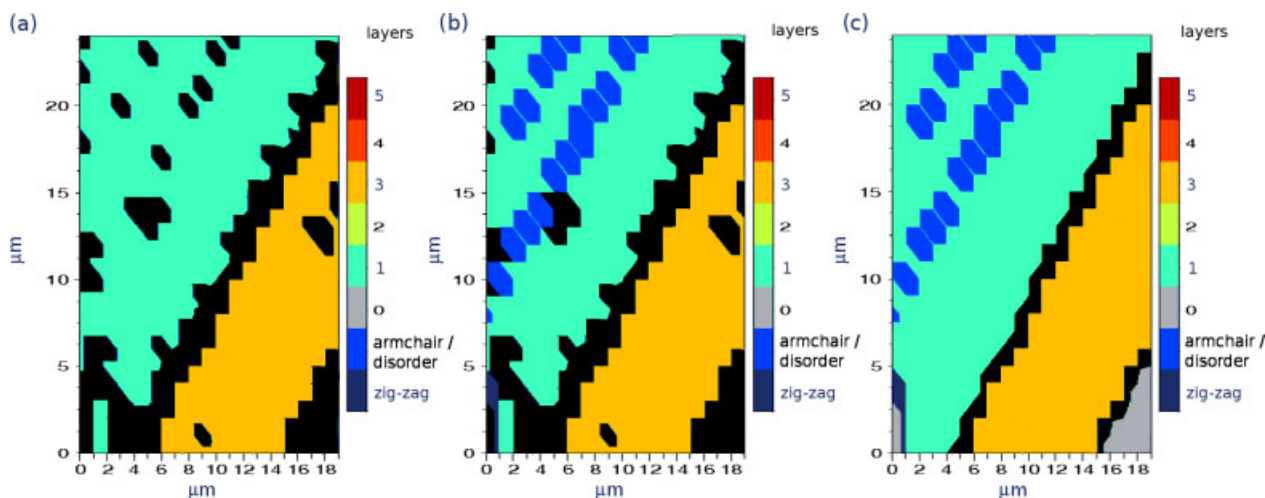**Figure 7.** Flowchart of the subroutine for the characterization of all positions.

Figure 8. Stages in the characterization process: (a) identification obtained by Int(G); second (b) edge composition is characterized by Int(G), 2D line and Int(D); (c) by fitting 2D band of previous unknown positions, some areas can be finally characterized.

the measurement, etc.), or when the scanned position is on the border between FLG and substrate, where the Int(G) is low due to the fact that the laser spot takes FLG and substrate area and the 2D peak cannot be fitted to one Lorentzian peak (as would correspond to graphene)).

(iii) If the position is not in the border, its 2D band will be fitted to the two nearest values in IntCalc(G). If the 2D band fits to any of them, the position will be characterized; if not, there is a contradiction between G and 2D band values (might be due to spikes during the measurement), and the position will be established as 'uncharacterized position'.

Figure 8 represents the three stages within the characterization subroutine for the area presented in Fig. 1(a). Identification through Int(G) (Fig. 8(a)) presents some uncharacterized areas (black areas). Then, positions belonging to border places are identified via Int(D) (Fig. 8(b)). Finally, in the case of having 'uncharacterized positions', still 2D band fittings (Fig. 8(c)) are performed to identify them if possible.

In Fig. 9, we show the program results for the scanned areas presented in Fig. 1. As already mentioned, we used the AFM results to prove the efficiency of the algorithm. We have tested the algorithm for several samples and it was able to characterize most positions within the mapping (roughly we have employed
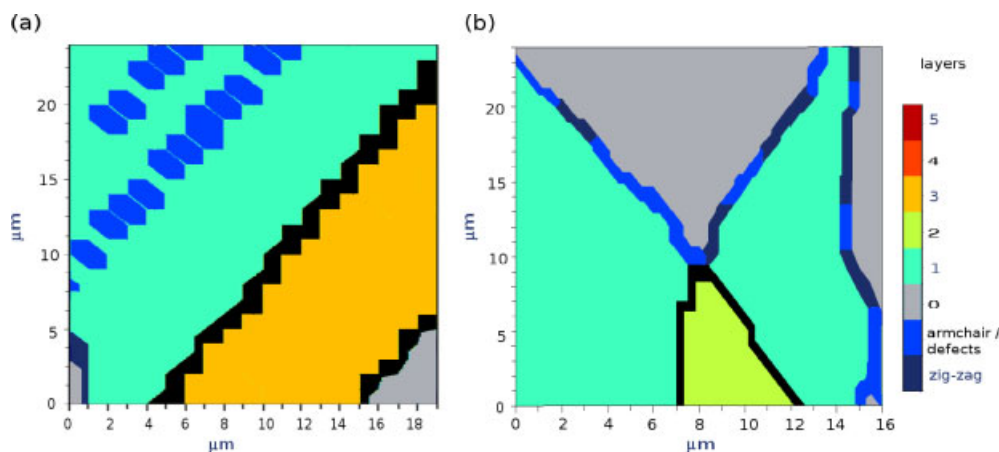
Figure 9. Final characterization of the areas presented in Fig. 1. The final uncharacterized regions (black pixels) are those in which the laser spot is incident simultaneously in two zones (graphene–FLG, FLG–substrate or FLG–FLG).

the algorithm for more than 20 000 Raman spectra producing satisfactory results in approximately 90% of cases). Computation time for data processing of 500 spectra is around 2 min (data processing was undertaken in a 1-GHz processor desktop). Furthermore, as shown in Fig. 9, most of the 'uncharacterized positions' remaining at the end of the program correspond to transitions graphene–FLG, FLG–substrate or FLG–FLG.

Conclusion

In conclusion, we have presented an algorithm that undertakes a basic but robust characterization of graphene and FLG by selecting and combining appropriate parameters of the Raman spectra. This identification method can be used for any type of substrate. The possibility of having an efficient automatic detection and characterization method for graphene and FLG is vital in order to be able to use this promising material for industrial applications and nanodevices. Moreover, the algorithm can be continuously upgraded simultaneously as Raman studies on graphene go further. For example, some improvements can be introduced using the information shown in Fig. 5 to select and detect the quality of graphene, i.e. disorder and doping levels.

Acknowledgements

References

[1] K. S. Novoselov, A. K. Geim, S. V. Morozov, D. Jiang, Y. Zhang, S. V. Dubonos, I. V. Grigorieva, A. A. Firsov, *Science* **2004**, *306*, 666.
[2] A. H. Castro Neto, F. Guinea, N. M. R. Peres, K. S. Novoselov, A. K. Geim, *Rev. Mod. Phys.* **2009**, *81*, 109.
[3] A. K. Geim, K. S. Novoselov, *Nat. Mater.* **2007**, *6*, 183.
[4] C. Berger, Z. Song, T. Li, X. Li, A. Y. Ogbazghi, R. Feng, Z. Day, A. N. Marchenkov, E. H. Conrad, P. N. First, W. A. de Heer, *J. Phys. Chem. B* **2004**, *108*, 19912.
[5] C. Oshima, A. Nagashima, *J. Phys. C* **1997**, *9*, 1.
[6] R. Rosei, S. Modesti, F. Sette, *Phys. Rev. B* **1984**, *29*, 3416.
[7] S. Stankovic, D. A. Dikin, G. H. B. Dommett, K. M. Kohlhass, E. J. Zimney, E. A. Stach, R. D. Piner, S. T. Nguyen, R. S. Ruoff, *Nature* **2006**, *442*, 282.
[8] S. Roddaro, P. Pingue, V. Piazza, V. Pellegrini, F. Beltram, *Nano Lett.* **2007**, *7*, 2707.
[9] T. Ohta, A. Bostwick, T. Seyller, K. Horn, E. Rotenberg, *Science* **2006**, *313*, 951.
[10] M. H. Yan, B. zyilmaz, Y. Zhang, P. Kim, *Phys. Rev. Lett.* **2007**, *98*, 206805.
[11] A. Geim, *Science* **2009**, *324*, 1530.
[12] P. Blake, E. W. Hill, A. H. Castro Neto, K. S. Novoselov, D. Jiang, R. Yiang, T. J. Booth, A. K. Geim, *Appl. Phys. Lett.* **2007**, *91*, 063124.
[13] Z. H. Ni, H. M. Wang, J. Kasim, H. M. Fan, T. Yu, Y. H. Wu, Y. P. Feng, Z. X. Shen, *Nano Lett.* **2007**, *7*, 2758.
[14] I. Jung, M. Pelton, R. Piner, D. A. Dilkin, S. Stankovich, S. Watcharotone, M. Hausner, R. S. Ruoff, *Nano Lett.* **2007**, *7*, 3569.
[15] L. Gao, W. Ren, F. Li, H. Cheng, *ACS Nano* **2008**, *2*, 1625.
[16] A. Gupta, G. Chen, P. Joshi, S. Tadigadapa, P. C. Eklund, *Nano Lett.* **2006**, *6*, 2667.
[17] C. Casiraghi, A. Hartschuh, E. Lidorikis, H. Qian, H. Harutyunyan, T. Gorkus, K. S. Novoselov, A. C. Ferrari, *Nano Lett.* **2007**, *7*, 2771.
[18] P. Nemes-Incze, Z. Osv'ath, K. Kamar'as, L. P. Biró, *Carbon* **2008**, *46*, 1435.
[19] M. Ishigami, J. H. Chen, W. G. Cullen, M. S. Fuhrer, E. D. Williams, *Nano Lett.* **2007**, *7*, 1643.
[20] J. C. Meyer, A. K. Geim, M. I. Katsnelson, K. S. Novoselov, T. J. Booth, S. Roth, *Nature* **2007**, *446*, 60.
[21] K. A. Ritter, J. W. Lyding, *Nanotechnology* **2008**, *19*, 015704.
[22] U. Stberl, U. Wurstbauer, W. Wegscheider, D. Weiss, J. Eroms, *Appl. Phys. Lett.* **2008**, *93*, 051906.
[23] A. C. Ferrari, J. C. Meyer, V. Scardaci, C. Casiraghi, M. Lazzeri, F. Mauri, S. Piscanec, D. Jiang, K. S. Novoselov, A. K. Geim, *Phys. Rev. Lett.* **2006**, *97*, 187401.
[24] D. Graf, F. Mollitor, K. Ensslin, C. Stampfer, A. Jungen, F. Mauri, C. Hierold, L. Wirtz, *Nano Lett.* **2007**, *7*, 238.
[25] Y. M. You, Z. H. Ni, T. Yu, Z. X. Shen, *Appl. Phys. Lett.* **2008**, *93*, 163112.
[26] C. Casiraghi, A. Hartschuh, H. Quian, S. Pisanec, C. Georgi, A. Fasoli, K. S. Novoselov, D. M. Basko, A. C. Ferrari, *Nano Lett.* **2009**, *9*, 1433.
[27] A. K. Gupta, T. J. Russin, H. R. Guti'errez, P. C. Eklund, *ACS Nano* **2008**, *3*, 45.
[28] C. Casiraghi, S. Pisana, S. NovoselovK, A. K. Geim, A. C. Ferrari, *Appl. Phys. Lett.* **2007**, *91*, 233108.
[29] Z. H. Ni, T. Yu, Z. Q. Luo, Y. Y. Wang, L. Liu, C. P. Wong, J. Miao, W. Huang, Z. X. Shen, *ACS Nano* **2009**, *3*, 569.
[30] A. C. Ferrari, *Solid State Commun.* **2007**, *143*, 47.
[31] I. Calizo, D. Teweldebrhan, W. Bao, F. Miao, C. N. Lau, A. A. Baladin, *J. Phys. Conf. Ser.* **2008**, *109*, 012008.
[32] Y. Y. Wang, Z. H. Ni, T. Yu, Z. X. Shen, H. M. Wang, Y. H. Wu, W. Chen, A. T. S. Wee, *J. Phys. Chem. C* **2008**, *112*, 10637.
[33] S. Gandhi, *VLSI Fabrication Principles*, John Wiley and Sons: New York, **1983**.

[34] I. Calizo, A. A. Balandin, W. Bao, F. Miao, C. S. Lau, *Nano Lett.* **2007**, *7*, 2645.

[35] C. Castiglioni, M. Tommasini, G. Zerbi, *Philos. Trans. R. Soc. Lond. A* **2004**, *362*, 2425.

[36] Z. Hua Ni, T. Yu, Y. Hao Lu, Y. Ying Wang, Y. Ping Feng, Z. Xiang Shen, *ACS Nano* **2008**, *2*, 2301.

[37] C. Casiraghi, *Phys. Stat. Sol. RRL* **2009**, *3*, 175.

[38] Y. Y. Wang, Z. H. Ni, Z. X. Shen, *Appl. Phys. Lett.* **2008**, *92*, 043121.

[39] J. S. Park, R. Saito, J. Kong, G. Dresselhaus, M. S. Dresselhaus, *Carbon* **2009**, *47*, 1303.

[40] L. C. Cançado, A. Reina, J. Kong, M. S. Dresselhaus, *Phys. Rev. B* **2008**, *77*, 245408.